

Dynamic Stray Current Evaluations on Cut-and-Cover Sections of DC Metro Systems

C. A. Charalambous, *Member IEEE*, P. Aylott

Abstract— The tunneling construction in underground DC Metro Systems is mainly based on the Bored Tunnel Method and the Cut-and-Cover method. Therefore the stray current assessments and mitigation actions should be tailored according to which method of tunnel construction is used. This paper presents a topologically-accurate model to assess the dynamic stray current picture in cut-and-cover sections of DC metro systems. The dynamic stray current evaluation can provide an indication to the extent of the corrosion problem in the supporting and third party infrastructure of the system. In this work the dynamic evaluations are based on a combination of various ideal and realistic train operation scenarios.

Index Terms— DC Transit Systems, Stray Current Design and Control, Cut-and-Cover Systems, Dynamic Modeling

I. INTRODUCTION

THE tunneling construction in underground DC Metro Systems is mainly based on the Bored Tunnel Method (B.T.M) and the Cut-and-Cover Method. Cut-and-cover tunneling is a relatively simple construction method used to build shallow tunnels. There exist three main construction methods for cut-and-cover tunnels, namely, the conventional method, the bottom-up method and the top-down method (or diaphragm wall method) [1]. Each of these methods has its own construction characteristics; however their common feature is the backfilling of an excavated trench to restore the roadway or ground on top of the tunnel.

Materials used, to provide the structure and support in the construction of cut-and-cover tunnels, may include reinforced concrete, pre-cast concrete or corrugated steel arches. In contrast, the reinforcement in adjoining segments (both circumferential and longitudinal) in Bored Tunnel Systems (B.T.S) may be bolted together through PVC sleeves. Therefore the tunnel segments in B.T.S are not electrically continuous, as opposed to the electrically continuous tunnel structures in cut-and-cover sections.

This difference in tunnel construction method constitutes a major factor that should be reflected in the stray current

assessment of DC metro systems. As detailed in [2], for a Bored Tunnel System (B.T.S.) the primary stray current corrosion risk is to the rails and their fixings and partly to the tunnel walls (should these become continuous through the tunnel services).

However, when approaching the stray current design for cut-and-cover sections, the impact on the tunnel structure itself should be carefully assessed because of its inherent electrical continuity. Moreover, the spread of stray current in other parts of the system (embraced by the cover-and-cover sections) should also be examined. It is noted that corrosion will occur at each point that current transfers from a metallic conductor, such as a reinforcement bar in concrete, to the electrolyte (i.e. the concrete). Hence stray current leakage can cause corrosion damage to the rails, the tunnel reinforcement and to third party systems such as external buried pipework. Severe damage may occur as a result of stray current leakage [3].

To address these specific requirements, this paper presents a topologically accurate model to assess the dynamic stray current picture in cut-and-cover sections of DC metro systems. The dynamic evaluation is based on a combination of ideal and realistic train operation scenarios. The design data and characteristics of the cut-and-cover section modeled are taken from a real system currently under construction.

A. Contributions beyond the State-of-the Art

Existing railway stray current model applications have the ability to compute rail voltage to remote earth and current flow in the modeled third party components under various scenarios dependent upon their design [4]-[6].

Railway stray current flows are also modeled in response to multiple train position [7] and of train regeneration characteristics [8]. The impacts measured on affected structures and services present the net effect of variable factors such as two-tracks cross bonding, soil resistivity and soil structure [9]. On some occasions the current impact assessments are limited to simple time averaging and linear extrapolation of current flows from either static or dynamic model outputs. Some dynamic simulations are presented in [10]-[12] in an attempt to investigate the effect of three different earthing schemes (floating, solidly bonded and diode bonded) on rail potential and produced stray currents. These simulations were mounted on a resistive type network (to account for the rails and the stray current collection grid) and consider some of the trains' performance characteristics and data.

In view of the above contributions, the work presented in this paper reinforces the existing stray current modeling endeavours by providing the following advancements over the

"Copyright (c) 2013 IEEE. Personal use of this material is permitted. However, permission to use this material for any other purposes must be obtained from the IEEE by sending a request to pubs-permissions@ieee.org." C.A. Charalambous is with the Department of Electrical and Computer Engineering of University of Cyprus, PO Box 20537, 1687, Nicosia, Cyprus (e-mail: cchara@ucy.ac.cy). Pete Aylott is with Intertek, Manchester M1 7DP, U.K. (e-mail: pete.aylott@intertek.com).

existing methods: *a) Assess the stray current performance of Cut-and-Cover sections of DC metro systems:* The method and models developed can both cumulatively and topologically evaluate the stray current performance of the complex 3D geometry and specific design characteristics of cut-and-cover tunnel systems.

b) Assess the dynamic stray current picture of all elements embraced in a cut-and-cover tunnel: The model computes the dynamic stray current performance and provides an indication to the extent of the corrosion problem in all the supporting and third party infrastructure of the system. In this work the dynamic evaluation is based on a combination of ideal train operation modes as well as on a sample of a realistic train operation. *c) Dynamical Assessment of the maximum longitudinal voltage drop caused by operation in the tunnel:* Current standards (e.g. EN 50122-2 and 50162) apply criteria based on exceedance of absolute or averaged corrosion potential thresholds without regard to current flows. To facilitate this, the model computes time-varying voltages at various monitoring locations on the tunnel and on the third party infrastructure. This is done to accommodate assessments regarding the maximum allowable potential value - dictated by EN 50122-2 [13]. It is one of the key developments of this work as it ties electrical simulations of the railway to corrosion effects on services.

II. FUNDAMENTAL MODELING PRINCIPLES

Fig. 1 illustrates a cross-section of a cut-and-cover section in its actual dimensions. The tunnel must be of sufficient size to accommodate all operational requirements and provision for services, fittings and furniture as required.

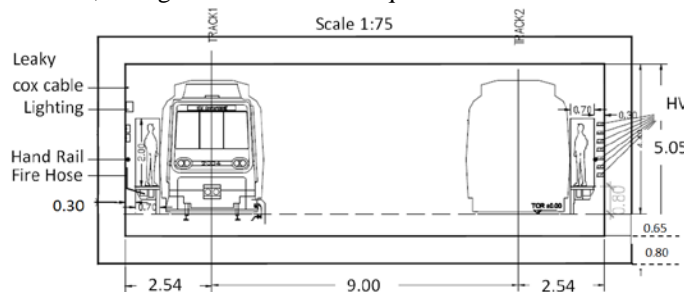


Fig. 1. Cross Section of a realistic two-track, Cut-and-Cover Tunnel with actual dimensions in m.

A. Characteristics of Base Simulation Model

A custom simulation model is formulated to represent all the possible current-return circuit elements of a cut-and-cover section. The ideal computer model formulated for a realistic 3D cut-and-cover section is illustrated in perspective view in Fig. 2 and in plan-view in Fig. 3. This is materialized within [14] following an assessment of the infrastructure elements considered to contribute to the stray current performance of the cut-and-cover systems. The software employs a Cartesian coordinate system with three coordinates (x, y, z), thus allowing the formation of topologically accurate simulation models, through the use of conductors. The arrangement of conductors is specified by virtue of their energisation method, the magnitude of the energisation, their material coating characteristics and the coordinates of each conductor along with its radii and number of specified segments. The

conductors segments can be subsequently associated with various energisation types (potentials, current injections and current flows).

In particular, Fig. 2 models a 1km section of a system, containing a single track (two rails) and a Stray Current Collection System (S.C.C.S) which embraces a Stray Current Collection Grid (S.C.C.G) and a Stray Current Collection Cable (S.C.C.C). It also models a metallic coated pipe (that serves the scope of assessing the effect of stray current on samples of the metallic infrastructure that lie in the nearby vicinity of the tunnel system) and a conductor-based, equivalent representation of the tunnel services. The tunnel walls of the cut-and-cover section are also modeled, using a set of conductors to represent reinforced concrete that is able to withstand aggressive soil and water conditions.

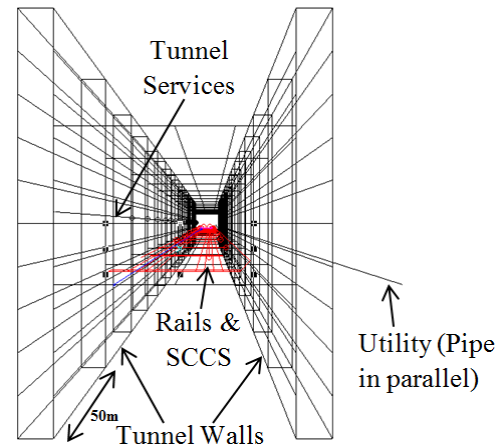


Fig. 2. Perspective view (3D) of the arrangement of conductive elements in the cut-and-cover simulation model

The plan view of the model (Fig. 3) illustrates in more detail the arrangement of each of the elements (e.g. rails, S.C.C.S, tunnel walls, pipe, and services) considered. The Stray Current Collection System (S.C.C.S) has been realised in the developed model as a geometric replicate of the system illustrated in Fig. 4. Furthermore, Fig. 3 illustrates the surrounding soil/ environment incorporated to approximate a shallow tunnel such as those used in the cut-and cover sections of underground Metro Stations.

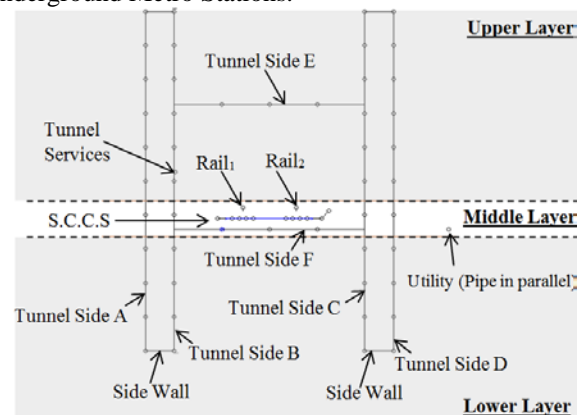


Fig. 3. Plan view of the arrangement of conductive elements and the soil layer models

The upper layer of the soil model is assigned a high resistivity of $10^{14} \Omega \text{ m}$, to eradicate any leakage current to flow from the rail track to the tunnel and tunnel services in an

upward direction. With this arrangement, any leakage current that would influence both the tunnel and its services could find its route path through the tunnel structure that sits within the concrete layer (middle layer). The structure of the soil model approximates the real situation and is computationally stable. To this end, a portion of the tunnel structure is situated in the middle soil layer which is assigned a resistivity of $180 \Omega \cdot m$ [2]. This represents the concrete present within the tunnel. The middle soil layer also embraces the running rails and the S.C.C.S (Fig. 4). Current from the running rails must flow through concrete to reach the collection grid or alternatively the tunnel reinforcement and services. It must also pass through the concrete to reach the surrounding soil. In this paper the lower layer of the soil model is assumed to have a resistivity of $15 \Omega \cdot m$.

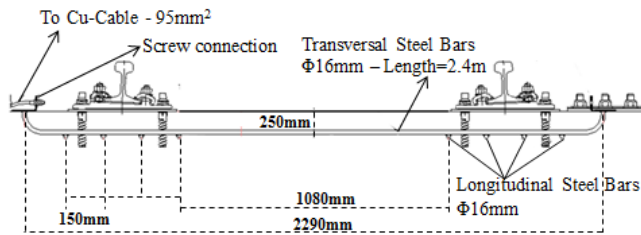


Fig. 4. Perspective view of the stray current collection system (S.C.C.S.)

With reference to Figs. 2-4 the modeled items of the stray current return circuit are now described in more detail: The two rails are modeled as UIC54 conductors having a longitudinal resistance of $40 \text{ m}\Omega$ per kilometer. The effect of discrete insulator pads is modeled by assuming the rails are coated with a resistive layer. This coating is set accordingly (by adjusting its thickness and resistivity) to account for a resistance to earth $100\Omega \cdot \text{km}$ single rail.

The S.C.C.S. consists of the Stray Current Collection Grid (S.C.C.G.) and the Stray Current Collection Cable (S.C.C.C.). The S.C.C.G. employs steel bars which are longitudinally placed under each rail (4 steel bars x $\Phi 16 \text{ mm}$ for each running rail - that is 2×4 steel bars x $\Phi 16 \text{ mm}$ for a single track as is shown in Fig. 4). This design provides an overall S.C.C.G. cross-section of 1608 mm^2 per track. The Stray Current Collection Cable (S.C.C.C) is bonded to the S.C.C.G. through flexible bare cables at 100 m intervals. Both cables are made from copper and their size is taken in the model as 95 mm^2 . The cables are insulated.

The tunnel services are modeled as a galvanized steel conductor to represent an overall tunnel service cross-sectional area of 79 mm^2 , equating to a conductor radius of 5 mm . The tunnel services are continuous but insulated from the tunnel walls. The pipe is modeled as a metallic (heavy duty galvanized steel) coated conductor.

The cut-and-cover tunnel structure is modeled as being electrically continuous. The model consists of four sets of vertically placed conductors to model the two side walls of the tunnel (Fig. 3). Each side wall consists of two sets of 11 conductors that are longitudinally extended along the 1 km section of the system (Tunnel Sides A, B, C, D). At 50 m intervals (Fig. 2) there is an electrical/ mechanical connection between each set of conductors on each side wall. The model also consists of an upper (Tunnel Side E) and a lower set

(Tunnel Side F) of 20 transversely spaced conductors (every 50 m) to simulate the top and bottom sections of the tunnel. These sets of conductors serve the scope of providing both structural support and electrical continuity within the tunnel. Moreover, within the simulation model, the tunnel conductors that sit outside the middle layer (concrete) are given a coating layer to emulate an artificial presence of concrete. This technique provides a method of modeling steel reinforced concrete that can be placed in different soil environments [15].

Finally, Table I summarises the base input data and assumptions employed in the subsequent simulations for assessing the stray current performance of the cut-and-cover design.

TABLE I
BASE INPUT DATA AND ASSUMPTIONS

Parameter	Value
Track length & power supply	1 km single track with a supply substation at either end.
Rail resistance	$40 \text{ m}\Omega/\text{km}$ (UIC54)
Rail conductance** (resistance to earth)	$100 \Omega \cdot \text{km}$
Soil Model Resistivity	Upper: $10^{14} \Omega \cdot \text{m}$ Middle: $180 \Omega \cdot \text{m}$ (Concrete) Lower: $15 \Omega \cdot \text{m}$
Soil Model Width	Upper: 5.8 m Middle: 1 m (Concrete) Lower: Infinite
Stray Current Collection Grid (S.C.C.G.)	2×4 steel bars x $\Phi 16 \text{ mm}$ for a single track
Stray Current Collector Cable (S.C.C.C)	95 mm^2 - copper - bonded to S.C.C.G. at 100 m intervals
Stray current collector cable termination at substations	Floating
Tunnel Reinforcement and Coating	$\Phi 20 \text{ mm}$ - Steel (Sides A, B, C, D) $\Phi 30 \text{ mm}$ - Steel (Sides E, F) Coating: $180 \Omega \cdot \text{m}$ (where appropriate)
Tunnel Dimensions	Height: 9.5 m Width: 6.92 m Length: 1000 m Distance of rooftop from ground level: 0.5 m
Tunnel Services	79 mm^2 - galvanized steel
Insulation of internal tunnel infrastructure (handrail, fire main etc.) from tunnel reinforcement	insulated
Utility (pipe in parallel)	1963 mm^2 - galvanized steel
** Driven by design and construction targets.	

B. Static Analysis and Benchmarking

A static version of the model presented in Fig.2 and Table I is simulated to confirm the validity of the model. The numerical results for the rail potential to earth as well as for the earth leakage current are shown in Fig. 5. These represent the worst static case scenario in terms of stray current performance evaluation (a single train at the center drawing the expected maximum average/RMS traction current (e.g. 2000 A) and a substation at each end each collecting it (e.g. 1000 A).

Based on the simulated results (Fig.5) the total positive stray current generation from the rails calculated by the model is 50.93 mA . This value may be confirmed by simple calculations when taking 2000 A (traction current) equally returning through a section of 500 m of two rails (i.e. 1000 A on each side) with a resistance of $40 \text{ m}\Omega/\text{km}$ of rail and a resistance to earth of $100 \Omega \cdot \text{km}$ (e.g. design recommendation). To further validate the model's output, the total generated stray current is calculated using a validated resistive-type model [7]. A benchmarking comparison (Total Stray Current) is tabulated in Table II.

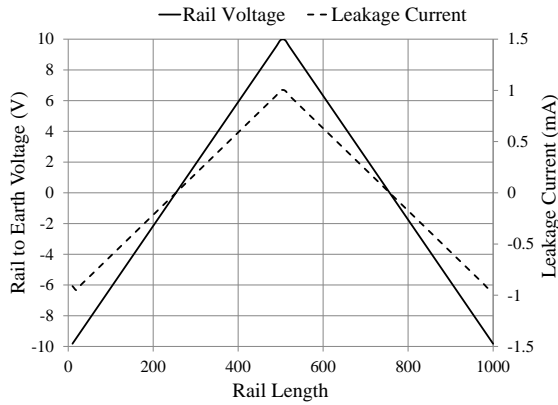


Fig. 5 Simulated Rail to Earth Voltage and Leakage Current (Rail I)

TABLE II
STRAY CURRENT CALCULATION BENCHMARKING

Total Stray Current		
Hand Calculations	Resistive Type Model [7]	Model Fig.2
50mA	49.95mA	50.1 mA

It is highlighted that a determination of the stray current levels under real life conditions can be achieved by applying scaling factors to the model results of Table II. A variation in track current will linearly influence the leakage current distribution due to the resulting alteration of rail-to-earth potential. Moreover, the rail to earth potential is determined by the currents flowing through the rail. Unless there is significant leakage that causes a change in the rail current flow, the leakage current density is proportional to the resistance of the rail insulation. The stray current influence resulting from the variation in a) the rail to earth resistance and b) the current drawn by the train is tabulated in Table III. The tabulated values are provided by the static version of the model presented in Fig.2 and Table I (albeit with varying rail to earth resistance values and load currents).

TABLE III

CALCULATED STRAY CURRENT LEVELS UNDER DIFFERENT RAIL TO EARTH RESISTANCE CONDITIONS FOR STATIC LOADS 2000A, 4000, 6000A (FLOATING SYSTEM)

Rail to earth resistance Ω km single track	Stray current with single train drawing 2000 A at 500m from each substation	Stray current with single train drawing 4000 A at 500m from each substation	Stray current with single train drawing 6000 A at 500m from each substation
EN 50122-2: permitted minimum: 2 Ω km	2.52 A	5.04 A	7.57 A
Design Recommendation: 100 Ω km	50.1 mA	100.63mA	150.12 mA
Service Operation: 40 Ω km	125.34 mA	250.21 mA	37.38 mA

III. PRINCIPLES OF DYNAMIC MODELING

The dynamic model is articulated with the aid of a commercially available software platform [16] interfaced to the 3D cut-and-cover section realized within [14] (Section II). This interface is necessary to facilitate time-variable current flows in the 3D topology of the model shown in Fig. 6. The current flows come in response to various train mode operations as a function of dynamic changes in multiple train

positions and speed modes along the 1km cut-and-cover section modeled.

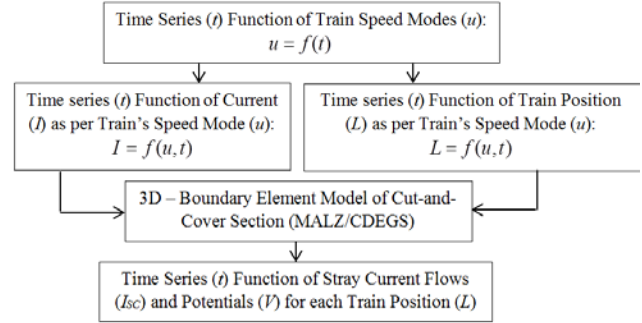


Fig. 5. Fundamental Principle of Dynamic Simulations

The first stage of the computation process (i.e. computation of currents drawing by the train) relates to a change in the train's operation speed over time, across the 1km length of the tunnel. This computation process involves the use of equations of motions and laws of physics applicable to train movement as well as electric machines/drives theory to determine the correlation of train's current needs to each operation mode, as described in [17]. More specifically, the train's relative position (L_n) is calculated as function (1) of train's varying speed (U_n) at any given instant in time (t_n).

$$L_n = f(U_n, t_n) \quad (1)$$

Thus the corresponding traction current (I_n) is calculated as a function (2) of the train's varying speed (U_n), which is in turn a function of the train's position (L_n) at time (t_n).

$$I_n = f(U_n) \rightarrow I_n = f(L_n, t_n) \quad (2)$$

Following these principles, two ideal and one realistic scenario are modeled in this paper: A) *Constant Torque Load*, B) *Constant Acceleration Load*, C) *Realistic Load*. Figure 7 illustrates the variation of traction current along the 1km tunnel length for each of the scenarios modeled. It is noted that with constant torque loads (Scenario A) the torque loading is not a function of speed. As the speed changes, the load torque remains constant and the power may change linearly with speed [17]. Scenario C illustrates a current profile that reflects on a realistic case as it combines various modes of operation including brake-deceleration.

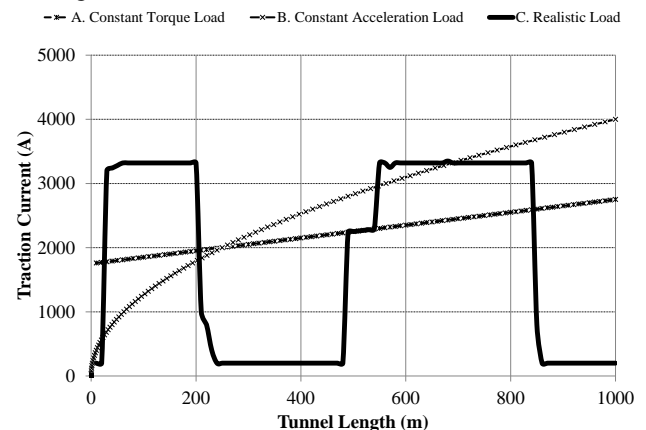


Fig. 7. Variation of Traction Current along the Tunnel Length

The traction current (I_n) computed in (2) is subsequently injected to the 3D cut-and-cover system developed. It should be noted that the injection of the traction current is an artificial representation of the 3rd rail conductor circuits. It is based on

current sources/ sinks, modeled in such a way to represent the current return flow to the supplying substations, depending on the train's relative location and speed mode. Hence, the software's module allows currents to be monitored at various points set on the network of conductors (Fig. 2). It further computes the flow of stray currents (I_{sc}) and voltages (V) for each individual conductor segment within the network.

The current injection process is simultaneously performed at time steps (t) determined by the train's location (L) and speed mode (U) within the 1km section modeled. This concept is formulated as a matrix (see Fig. 8) to illustrate the interdependencies in the subsequent dynamic stray current calculations (I_{sc}).

	t_1	t_2	t_m
L_1	$I_{sc}(t_1, L_1)$	$I_{sc}(t_2, L_1)$	$I_{sc}(t_m, L_1)$
L_2	$I_{sc}(t_1, L_2)$	$I_{sc}(t_2, L_2)$	$I_{sc}(t_m, L_2)$
\vdots	\vdots	\vdots	\diagdown	\vdots
L_n	$I_{sc}(t_1, L_n)$	$I_{sc}(t_2, L_n)$	$I_{sc}(t_m, L_n)$

Fig. 8. Universal Illustration of the Matrix for Stray Current Calculations

The matrix is individually formulated, for each scenario of Fig. 7; separately for all sets of the conductor elements (e.g. rails, S.C.C.S, tunnel and services) of the system. The formulation considers: a) the train's position, b) the train's speed mode and c) a corresponding time step.

In simpler terms, while the train moves, various monitoring locations are selected (L_1, L_2, \dots, L_n) – along the tunnel - based on the time (t_1, t_2, \dots, t_n) needed for the train to reach them. At each location (e.g. L_1), an associated stray current profile is calculated for each time step. For example the first row of the matrix tabulates the stray current time variation - t_1 to t_m - at location L_1 .

Hence, a post processing tool is developed within [16] to dynamically evaluate the corrosive stray current (I_{csc}) for all the conductive elements embraced by the modeled cut-and-cover section. The corrosive leakage current is defined as the current leaking from a conductor to an electrolyte i.e. the positive values of I_{sc} . At each specific monitoring location, a total amount of positive leakage current is accumulated, over time, on a time stepping (t_k) basis. This is defined as the total corrosive stray current (I_{csc}) given in (3). It can be discretely calculated for the n of locations defined along the 1km section.

$$\begin{aligned}
 I_{csc}(L_1) &= \sum_{k=1}^m I_{csc}(t_k, L_1) \\
 I_{csc}(L_2) &= \sum_{k=1}^m I_{csc}(t_k, L_2) \\
 &\vdots \\
 I_{csc}(L_n) &= \sum_{k=1}^m I_{csc}(t_k, L_n)
 \end{aligned} \quad (3)$$

In (3) n defines the number of monitoring locations which are forced to coincide with the distinct train positions (i.e. L_1 to L_n – see Fig. 8) along the 1km section. Moreover, k defines the number of time steps and m the total time needed for the train to cover the 1km section. Furthermore, the gross leakage charge (Q_{lc}) is calculated at each location (L) by integrating the corrosive stray current (I_{csc}), within specified time limits, as given in (5).

$$\begin{aligned}
 Q_{lc}(L_1) &= \int_{t_1}^{t_2} I_{csc}(t, L_1) \\
 Q_{lc}(L_2) &= \int_{t_1}^{t_2} I_{csc}(t, L_2) \\
 &\vdots \\
 Q_{lc}(L_n) &= \int_{t_1}^{t_2} I_{csc}(t, L_n)
 \end{aligned} \quad (5)$$

The gross leakage charge can be subsequently used in assessing of the corrosion impacts across the system by simple applications of Faraday's laws to assess the cumulative mass of metal loss over the target operating period [18].

IV. SIMULATION RESULTS AND ANALYSIS

The 3D cut-and-cover model described in Section II is simulated under the dynamic principles of the method analyzed in Section III. The simulations are able to dynamically evaluate the stray current performance of the complex 3D geometry and the specific design characteristics of the system both topologically and cumulatively.

A. Stray Current Generation - Time Variation

Fig. 9 illustrates the calculated time variation of the generated stray current (I_{sc}) for scenario C (i.e. realistic load). For clarity, the graph illustrates the results captured at three monitoring locations (100m, 300m, and 700m) along the 1km rails section.

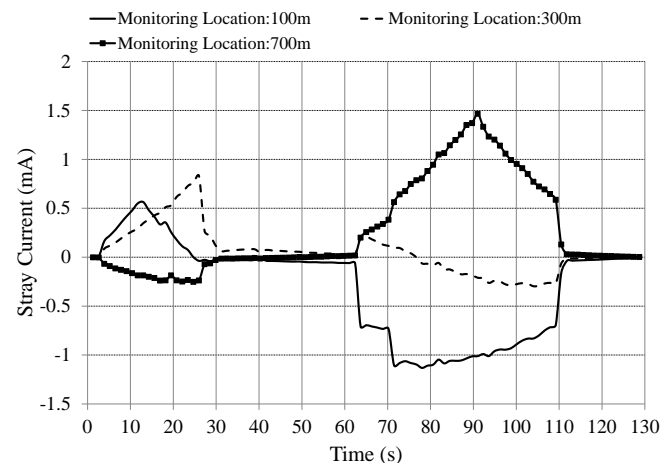


Fig. 9. Time Variation of Traction Stray Current at Various Monitoring Locations (on the rails) for Scenario C.

The results show that the time variation of the traction stray current is appropriately mirroring the shape of the traction load curve illustrated in Fig.7 as well as the train's location. For example, at monitoring location 700m, the stray current variation that is captured early in time (0-30s), is negative owing to the fact the train is far from the 700m observation point. However, its magnitude depends on the

traction load current occurring between 0-30s. Hence, by integrating the positive values of I_{sc} with time, in each graph, the gross leakage charge (Q_{lc}) may be calculated for each considered location (L).

Moreover, Fig. 10 illustrates a comparison of the calculated time variation of the generated stray current (I_{sc}) for all the scenarios shown in Fig. 7 – as monitored at 500 m along the 1km rail length. As in Fig. 9 the plots quantify how the time variation of the generated stray current is associated to the traction load current and location (depending on the train's mode of operation).

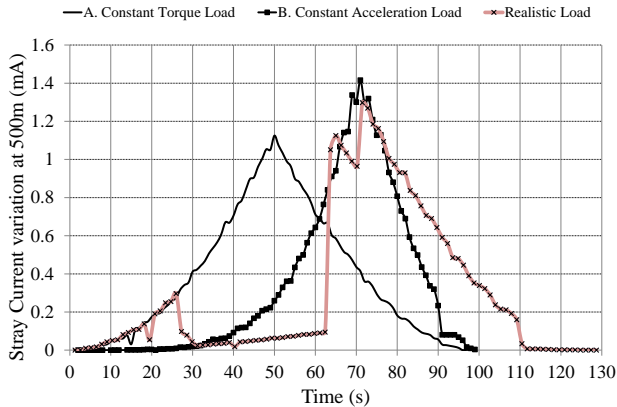


Fig. 10. Comparison of the Time Variation in Traction Stray Current for all scenarios modeled.

B. Topological Stray Current Dynamic Assessment

The topological stray current dynamic assessments serve the scope of illustrating the distribution of the gross leakage charge (Q_{lc}) at various locations (L) that associate with the rails, S.C.C.G, tunnel and pipe respectively. Fig. 11 illustrates a comparison of the Q_{lc} for the constant torque (A) and realistic load scenario (C). In both cases the calculation is based on 99 monitoring locations (i.e. every 10 meters). It is shown that the leakage charge is not evenly distributed along the rail length and may also depend on the mode of train operation (see the realistic load scenario charge curve – Fig. 9). Hence the corrosion risk will rise in regions where the accumulated gross leakage charge is higher.

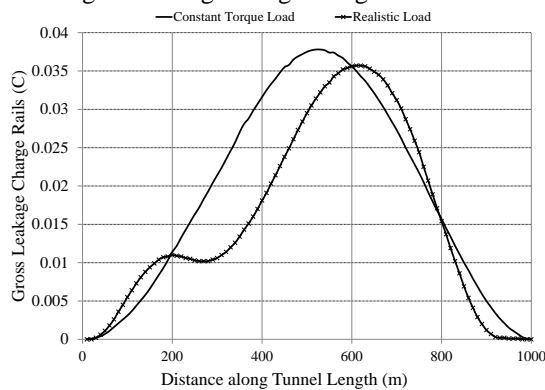


Fig. 11. Topological Assessment of Traction's Gross Leakage Charge for Scenario A and C

Moreover, Fig. 12 illustrates the simulated geometrically accurate 3D plot of the cumulative gross leakage charge profile (captured at 792 monitoring locations) of the Stray Current Collection Grid (S.C.C.G) for scenario A. The plot

suggests that the S.C.C.G is likely to suffer more stray current corrosive damage at its two ends. This seems rational, because the stray current is more probable to return back (through the surrounding soil) to the supplying substations which are usually located at the two side ends of the collection grid.

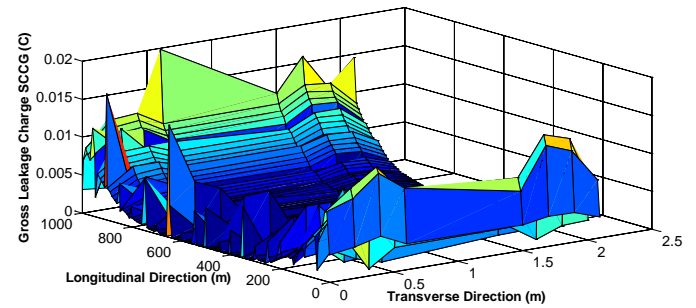


Fig. 12. Topological Assessment of S.C.C.G Gross Leakage Charge for Scenario A

Similarly, Fig. 13 illustrates the simulated geometrically accurate 3D plot of the cumulative gross leakage charge profile (captured at 400 monitoring locations) in one of the tunnel's side wall (Side Wall B – Fig. 3) for scenario A. The plot shows that, as in the case of the S.C.C.G, the sections of the tunnel that are closer to the supplying substations (i.e. the two ends of the tunnel) are more likely to be affected by the stray current activity.

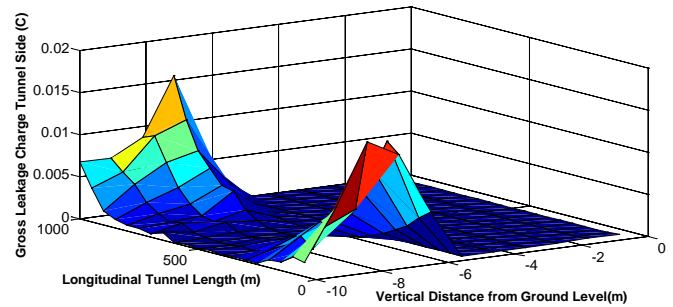


Fig. 13. Topological Assessment of Tunnel's Side Wall B Gross Leakage Charge for Scenario A

Finally Fig. 14 illustrates the calculated Gross Leakage Charge profile (captured at 99 monitoring locations) of the metallic coated pipe modeled (see Fig. 3) for scenario A.

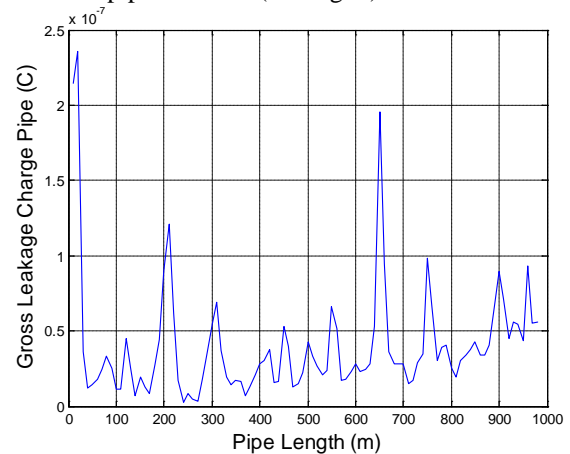


Fig. 14. Topological Assessment of Pipe's Gross Leakage Charge for Scenario A

In this case the stray current dynamic activity seems some dependency on the location of the supplying substations. There is an initial peak at <50m, and a higher trend level as it gets

closer to 1000m justifying some substation location dependency. It is possible that the metallic coated pipe can be exchanging stray currents with the tunnel infrastructure (since they run in parallel), making the picture more complex.

C. Cumulative Stray Current Dynamic Assessment

As previously noted the post-processing analysis is able to provide a cumulative assessment of the gross leakage charge (CQ_{lc}) for all the elements of the cut-and-cover section modeled. As an example, the CQ_{lc} is given as described in (6) for the case of rails. It is basically an index showing the cumulative effect of corrosive leakage current activity as collectively obtained by all monitoring locations ($L_1 - L_n$). The same approach (6) is followed for the other elements (e.g. S.C.C.G) of the system.

$$CQ_{lc}(\text{Rails}) = \int_{t_1}^{t_2} I_{csc}(t, L_1) + \int_{t_1}^{t_2} I_{csc}(t, L_2) + \dots + \int_{t_1}^{t_2} I_{csc}(t, L_n) \quad (6)$$

Table IV tabulates the cumulative gross leakage charge as calculated by the post processing tool developed. The tabulated results correspond to all scenarios illustrated in Fig. 7. They reflect on the relevant current-return conductors of the cut-and-cover tunnel system.

To facilitate a valid comparison the cumulative gross leakage charge, calculated in each scenario (Fig. 7), corresponds to the same number of monitoring locations (along the 1km sections of the cut-and-cover system). The same monitoring locations were chosen for all three scenarios examined in this paper.

TABLE IV
CUMULATIVE GROSS LEAKAGE CHARGE COMPARISON

Scenario:	Cumulative Gross Leakage Charge (C)		
	A	B	C
	Constant Torque	Constant Acceleration	Realistic Mode
Rails	3.76	3.34	3.15
S.C.C.G	2.42	2.36	2.014
Tunnel	0.86	0.81	0.78
Services	9.62e-005	6.70e-05	3.83e-005
Pipe	3.92e-006	3.73e-06	3.31e-006

The tabulated results are indicative and should be appropriately interpreted. For example, the cumulative charge (in all elements) observed for Scenario A is greater than the charge observed for Scenarios B and C respectively. This is due to the fact that the average current drawn by the train along the 1km section, is 2255 A for Scenario A, 2020 for Scenario B and 1840.7 A for Scenario C.

Thus, the above cumulative analysis may be used to justify the credibility of the static stray current modeling endeavours [2], [7]. The static evaluations usually use the expected maximum average/RMS traction return current value along the running rails, as the worst-case scenario for modeling the impact of stray current on the supporting and third-party infrastructure. Thus, the same conclusion (as in Table IV) can be reached, by static modeling, with regards to the cumulative effect of the dynamic stray current activity on the supporting infrastructure.

D. Stray Current Performance and Sensitivity Analysis

Table V tabulates the stray current performance of the system (Fig. 2) simulated under the static conditions stated in Section II-B. The system's performance has undergone a sensitivity analysis with the respect to the geometric design topology of the S.C.C.S. Figure 4 shows that under each rail four longitudinal steel bars are transversally spaced at a distance of 150 mm (i.e. a cross-section of 1608 mm² per track). The distance between the longitudinal steel bars has been varied to 50mm and 250mm respectively however the same effective cross-section area for the S.C.C.S is maintained, by keeping the same number of bars.

TABLE V
STRAY CURRENT PERFORMANCE AND SENSITIVITY ANALYSIS

	Distance between the longitudinal steel bars		
	50mm	150mm	250mm
Total Stray Current Rails (mA)	50.7 mA	50.1mA	50.2 mA
Efficiency of S.C.C.S (%)	73.77 %	79.04 %	81.69 %
Total Stray Current Tunnel (mA)	13.8 mA	8.969 mA	7.68 mA
Total Stray Current Pipe (mA)	0.0816mA	0.0615 mA	0.0518 mA

The results clearly show that stray current performance of the cut-and-cover system is influenced by the topological arrangement of the longitudinal steel bars forming the S.C.C.S. For example the efficiency of the S.C.C.S (i.e. its ability to collect the generated stray current) improves by 7.92% when the transverse space between the bars changes from 50mm to 250mm. Similarly the total stray current activity on the tunnel infrastructure and the pipe is reduced 44.35 % and 36.51 % respectively when comparing the 50mm case to the 250mm.

V. DYNAMICAL ASSESSMENT OF VOLTAGE DROP CAUSED BY TRAIN OPERATION

Some stray current related standards (e.g. EN 50122-2 and 50162) apply criteria based on exceedance of absolute or averaged corrosion potential thresholds without regard to current flows. To facilitate this, the model's outputs are post processed to compute time-varying voltages and voltage shifts at various monitoring locations on the tunnel and on the metallic coated pipe.

Figure 15 illustrates the computed dynamic variation of the pipe's voltage for scenario B (i.e. constant acceleration). The plot shows the voltage variation as calculated from a monitoring location set at 500m along the pipe's length. It is obvious that the voltage on the pipe is gradually increasing in time, following the train's speed mode and its subsequent stray current generation profile. As in Fig. 10 (for stray current generation), the maximum voltage on the pipe in the constant acceleration scenario appears at 70s.

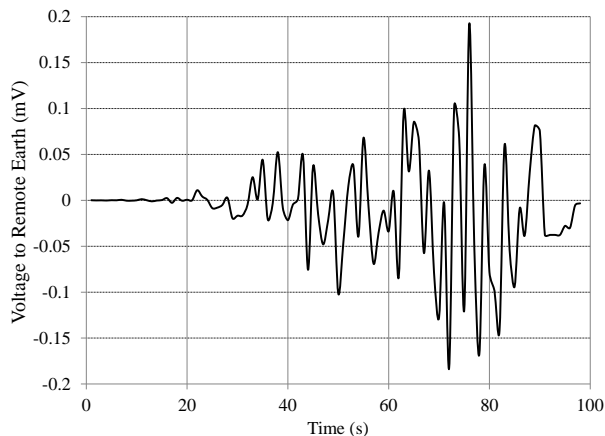


Fig. 15. Time Variation of Pipe's Voltage to Remote Earth for Constant Acceleration Scenario (Monitoring Location: 500m)

Moreover, the model is able to produce a time variation of the pipe's local voltage shift (V_{shift}) at specified monitoring locations (L) as shown in (7). The voltage shift is calculated as the difference in pipe's voltages to remote earth, at successive time steps.

$$V_{shift(L)}(t) = V_{remote_earth(L)}(t + t_{step}) - V_{remote_earth(L)}(t) \quad (7)$$

Thus, Figures 16 illustrate the calculations performed to assess the pipe's voltage shift (over time) for scenario C (realistic load) respectively. As in the previous case the assessment is carried out at a specific monitoring location (500m). It is shown that the local voltage shift is mirroring the shape of the traction load curve for the realistic load scenario (see Fig. 7). This behavior is found to be independent of observation point and to correspond with measurements made on operational systems [18].

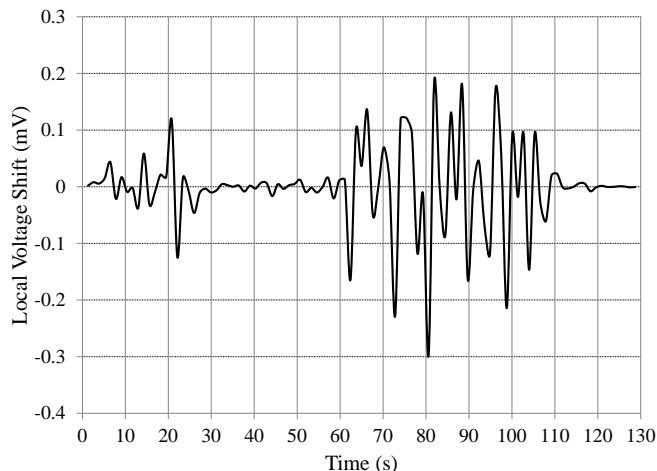


Fig. 16. Time Variation of Pipe's Voltage Shift for Realistic Load Scenario (Monitoring Location: 500m)

Finally, Fig. 17 shows the time variation of the voltage appearing on the conductors forming the tunnel side B (Fig. 3). The plot reflects on the realistic load scenario (C) considered in this paper. The monitoring location is also set at 500m.

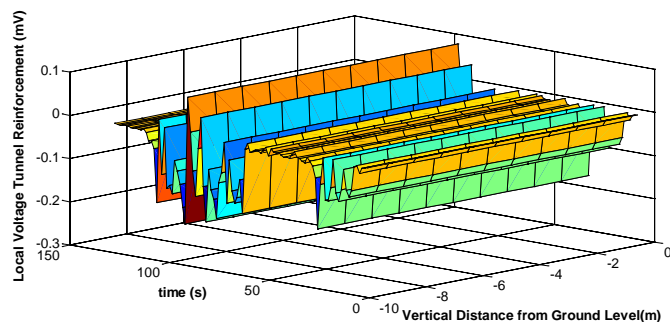


Fig. 17. Time Variation of Tunnel Reinforcement Voltage for Scenario C (Monitoring Location: 500m)

This calculation may be used as a benchmark to preliminary assess whether the proposed stray current design in the cut-and-cover system violates the maximum allowable potential shift - dictated by EN 50122-2 [13] for the longitudinal voltage drop caused by operation - in the tunnel reinforcement. Usually, the acceptance criteria for successful control of the tunnel's reinforcement potential shift are subject to a maximum limit of +0.2V (EN50162:2004 Table 1 [19]) from a reference potential value that is believed to prohibit corrosion.

VI. CONCLUSIONS

Although the paper has focused on cut-and-cover tunnel systems the method is directly translatable to other conditions such as bored tunnels and street railways which present a different mix of metallic conductors and soil or concrete environments while the general stray current behavior under these conditions can be inferred from cut-and-cover results. This benefits designers by highlighting the relative importance of the many different components that feed into stray current control and providing a method to compute likely impacts across their specific situation. More specifically the method allows designers to reassess some of the conservatism built into standards-based approaches and gives a method to assess realistic corrosion impacts under ideal and degraded conditions (such as reduced rail insulation conditions)

VII. REFERENCES

- [1] Available online at: <http://www.ametro.gr/page/default.asp?la=2&id=63>, Accessed on July 2013.
- [2] Charalambous, C.A.; Cotton, I.; Aylott, P.; Kokkinos, N.D., "A Holistic Stray Current Assessment of Bored Tunnel Sections of DC Transit Systems," Power Delivery, IEEE Transactions on , vol.28, no.2, pp.1048,1056, April 2013.
- [3] I. Cotton, C. Charalambous, P. Ernst, P. Aylott, "Stray Current Control in DC Mass Transit Systems", IEEE Transactions on Vehicular Technology, Vol. 54, No. 2, pages: 722 – 730, March 2005.
- [4] Dolara, A., Foadelli, F., Leva, S., "Stray Current Effects Mitigation in Subway Tunnels", Power Delivery, IEEE transactions on, On page(s): 2304 - 2311 Volume: 27, Issue: 4, Oct. 2012
- [5] Paul, D.; DC traction power system grounding, Industry Applications, IEEE Transactions on, Volume: 38, Issue: 3, May-June 2002, DC traction power system grounding, Pages: 818 – 824.
- [6] Pham, K.D.; Thomas, R.S.; Stinger, W.E.; "Analysis of stray current, track-to-earth potentials and substation negative grounding in DC traction electrification system" Railroad Conference, 2001. Proceedings.

- [7] Ogunsola, A.; Mariscotti, A.; Sandrolini, L. "Estimation of Stray Current From a DC-Electrified Railway and Impressed Potential on a Buried Pipe", *Power Delivery*, IEEE Transactions on Volume: 27 , Issue: 4, Digital Object Identifier: ,October 2012 , Page(s): 2238 – 2246.
- [8] Charalambous, C.A.; Cotton, I.; Aylott, P., "Modeling for Preliminary Stray Current Design Assessments: The Effect of Cross-track Regeneration Supply," *Power Delivery*, IEEE Transactions on , vol.28, no.3, pp.1899,1908, July 2013.
- [9] C. Charalambous, I. Cotton, "Influence of soil structures on corrosion performance of floating DC Transit Systems", *IET Research Journals - Electric Power Applications* (formerly IEE Proceedings), Vol. 1, Issue 1, pages: 9-16, January 2007.
- [10] Lee, C. -H.; Wang, H. -M.; Effects of grounding schemes on rail potential and stray currents in Taipei Rail Transit Systems, *Electric Power Applications*, IEE Proceedings-, Volume: 148, Issue: 2, March 2001, Pages: 148 – 154.
- [11] Hill, R.J.; Cai, Y.; Case, S.H.; Irving, M.R.; Iterative techniques for the solution of complex DC-rail-traction systems including regenerative braking, *Generation, Transmission and Distribution*, IEE Proceedings, Volume: 143, Issue: 6, Nov. 1996, Pages: 613 – 615.
- [12] C. A. Charalambous, I. Cotton, P. Aylott, "A simulation tool to predict the impact of soil topologies on coupling between a light rail system and buried third party infrastructure" , IEEE Transactions on Vehicular Technology, Vol. 57, No. 3, pages: 1404-1416, May 2008.
- [13] EN 50122-2: "Railway Applications – Fixed Installations – Electrical Safety, earthing and the return circuit – Part 2: Provisions against the effect of stray currents caused by d.c. traction systems", October 2010.
- [14] CDEGS Software, Safe Engineering Services & Technologies Ltd Montreal, Quebec, Canada Est. 1978.
- [15] Charalambous, C A; Cotton, I, "Stray current control and corrosion limitation for DC mass transit systems", Release date: 2011, Publisher: The University of Manchester. <https://www.escholar.manchester.ac.uk/uk-ac-man-scw:141928>).
- [16] MATLAB Release 2012a, The MathWorks, Inc., Natick, Massachusetts, United States.
- [17] SIU Lok Kee, "An Object-oriented railway system and power network simulator", PhD Thesis, University of Birmingham, UK, April 1995.
- [18] Aylott, P.J.; "Stray current is for life-not just for Christmas. Stray current corrosion management strategies for DC traction systems," *DC Traction Stray Current Control - Offer a Stray a Good Ohm?* (Ref. No. 1999/212), IEE Seminar on , Oct. 1999, pp.7/1-7/6.
- [19] EN-50162-2004; 'Protection against corrosion by stray current from direct current systems' August 2004.

VIII. BIOGRAPHIES

Charalambos A. Charalambous received a Class I BEng (Hons) degree in Electrical & Electronic Engineering in 2002 and a PhD in Electrical Power Engineering in 2006 from UMIST, UK. As of 2010, he is an Assistant Professor, in the Department of Electrical and Computer Engineering, at the University of Cyprus. Prior to this appointment he was with the Electrical Energy and Power Systems Group of the School Of Electrical and Electronic Engineering at the University of Manchester. His current research interests include power induced corrosion, Ferroresonance and Risk Management Applications in Power Systems.

Pete Aylott received the M.A. degree (Hons.) in natural sciences from the University of Cambridge, Cambridge, U.K., in 1981. Since 1985, he has been with CAPCIS Ltd (now part of Intertek Group plc), Manchester, U.K., where he is currently the Commercial Director. His consultancy experience covers the management of stray current on light rail and heavy rail underground systems and the interactions between these and the utility systems both across the U.K. and overseas.